

Ab initio calculation of ideal strength and phonon instability of graphene in tension

Fang Liu

*School of Applied Mathematics, Central University
of Finance and Economics, Beijing 100081, China*

Pingbing Ming

*LSEC, ICMSEC, Academy of Mathematics and Systems Science,
Chinese Academy of Sciences, Beijing 100080, China*

Ju Li*

*Department of Materials Science and Engineering,
Ohio State University, Columbus, Ohio 43210, USA*

Abstract

Graphene-based sp^2 -carbon nanostructures such as carbon nanotubes and nanofibers can fail near their ideal strengths due to their exceedingly small dimensions. We have calculated the phonon spectra of graphene as a function of uniaxial tension by density functional perturbation theory, to assess the first occurrence of phonon instability on the strain path, which controls the strength of a defect-free crystal at 0K. Uniaxial tensile strain is applied in x (nearest-neighbor) and y (2nd nearest-neighbor) directions, related to tensile deformation of zigzag and armchair nanotubes, respectively. The Young's modulus $E = 1050$ GPa and Poisson's ratio $\nu = 0.186$ from our small-strain results are in good agreement with previous calculations. We find that in both x and y uniaxial tension, phonon instabilities occur near the center of the Brillouin zone, at $(\varepsilon_{xx} = 0.194, \sigma_{xx} = 110$ GPa, $\varepsilon_{yy} = -0.016)$ and $(\varepsilon_{yy} = 0.266, \sigma_{yy} = 121$ GPa, $\varepsilon_{xx} = -0.027)$, respectively. Both soft phonons are longitudinal elastic waves in the pulling direction, suggesting that brittle cleavage fracture may be an inherent behavior of graphene and carbon nanotubes at low temperatures. *We also predict that a phonon band gap will appear in highly stretched graphene, which could be a useful spectroscopic signature for highly stressed carbon nanotubes.*

PACS numbers: 63.20.Dj, 62.20.-x, 81.05.Uw, 81.07.De

I. MOTIVATION

The ideal strength^{1,2} is the highest achievable strength of a defect-free crystal at 0K. Even though conventional materials deform or fracture at macroscopic stresses far below its ideal strength, the ideal strength is nonetheless a crucial theoretical parameter, because it fundamentally characterizes the nature of chemical bonding in that crystal^{3,4}. The Peierls-Nabarro model of dislocation^{5,6}, for instance, relies on the Frenkel model of ideal strength, because defects like cracks and dislocations work like levers, amplifying the far-field stress to near ideal strength levels inside the defect core, in order to move⁷. It is thus not surprising that the study of ideal strength can tell us a lot about why some materials (like diamond) are intrinsically brittle, while others (like copper) are intrinsically ductile⁴.

The ideal strength becomes even more important with the progress of nanotechnology. Recent experiments on nanocrystals⁸, nanoporous materials⁹, nanopillars¹⁰ and nanoindentation¹¹ have revealed a host of *ultra-strength* phenomena, defined by internal stress levels broadly and persistently rising up to a significant fraction of the ideal strength. Ultra-strength materials typically have geometric features around or less than $L_C \sim 10^2$ nm. To put this in perspective, computers one can buy off the shelf now have chips with 65 nm strained silicon features.¹² At such material lengthscales, the population dynamics of defects is fundamentally different from that in the macroscale material, leading to size-dependent mechanical behavior at $L > L_C$, which however starts to level off at $L < L_C$ due to the intrinsic upper bound, the ideal strength.

Carbon nanotube is an ultimate example of small-size, ultra-strength material. By bending multi-walled carbon nanotubes (MWCNTs) inside an atomic force microscope (AFM), Falvo et al. estimated that 16% tensile strain can be achieved in local regions of some MWCNTs without breaking them¹³. Yu et al. measured the tensile response of single-walled carbon nanotube (SWCNT) ropes¹⁴ and inferred a mean breaking strength of 30 GPa, 3% of their mean Young's modulus of 1002 GPa. Ding et al.¹⁵ measured the fracture strengths and moduli of arc-grown MWCNTs. The outer-shell fracture strength was estimated to range from 10 to 66 GPa, and the Young's modulus from 620 to 1200 GPa. Demczyk et al. conducted room-temperature pulling and bending tests on MWCNT of diameter 12.5 nm, and measured an astonishing 150 GPa failure strength, which is 17% of its Young's modulus $E = 900$ GPa¹⁶. The authors noted there is no narrowing of the nanotubes immediately before failure

(the deformation was elastic and reversible), and the nanotubes fail “as essentially defect-free materials”. The 150 GPa strength value however seems to be inconsistent with their reported 5% strain prior to failure. Barber et al.¹⁷ measured the tensile strength of MWCNTs produced by chemical vapor deposition and fit the data to Weibull-Poisson distribution. A characteristic strength value of 109 GPa was obtained. Marquez-Lucero et al. reported similarly high strengths in carbon nanotubes and nanofibers¹⁸. These recent experiments indicate that ultra tensile strength can indeed be achieved in an important component of nanotechnology.

It is reasonable to speculate that graphene-based carbon nanotubes, nanofibers, etc. hold record or near-record ideal *tensile* strength among all materials. It is well-known that the electronic structure and mechanical properties of carbon nanotubes are similar to those of flat graphene, aside from quantum confinement effect¹⁹. For this reason, in this paper we perform a careful ab initio study of the ideal tensile strength of flat graphene, as structural motif for carbon nanotubes, nanofibers and other graphene-based materials²⁰. The results we obtain for the ideal strain ε_I and ideal strength σ_I are expected to be directly comparable with experimental measurements for the carbon nanotubes^{13–17}.

II. METHODOLOGY

The ideal strength σ_I of a crystal is inherently related to its phonons^{21,22}. This is because at low temperatures (defined here as less than half the Debye temperature T_D , $T_D \sim 1000\text{K}$ in graphene²³), all atomic motions in the crystal can be decomposed into phonon modes, which are nearly independent of each other (normal modes). Therefore both the necessary and sufficient condition for mechanical instability of a crystal at low temperature is phonon instability^{24,25}, i.e., vanishing of the phonon frequency $\omega_{n\mathbf{k}}$ for some wavevector \mathbf{k} and branch index n . A mathematical understanding of this condition and its relation to the validity of Cauchy-Born rule relating stress to strain can be found in Ref. 26. A phonon mode that lowers the energy of a crystal (has imaginary frequency) will grow in amplitude, until nonlinearity kicks in and the structure is driven to a new stable state, often containing strain-relieving defects²⁵. The incremental atomic displacements of the unstable phonon mode can be determined from the eigenvectors of the dynamical matrix. The unstable eigenvector indicates the crystallographic nature of the initial instability. When free surfaces are under

load, the so-called surface ideal strength^{27,28} can also be calculated from surface phonon analysis²⁹.

Density functional perturbation theory (DFPT) is a well-tested ab initio method for accurate phonon calculations³⁰. Typical empirical interatomic potentials for semiconductors give up to 20% error in the calculated phonon frequencies at zero stress compared to experiments³¹, but one could usually expect $< 5\%$ error from parameter-free DFPT calculations³⁰. Furthermore, empirical interatomic potentials are fitted to mostly zero-stress properties; large-strain atomic environments leading to nonlinearity and bond breaking are often underrepresented in the fitting process. Therefore, empirical potential phonon calculations^{24,29} are useful for surveying the gross features of ideal strength, but are inappropriate for accurate predictions of ideal strength. The DFPT approach, on the other hand, does not have this problem. One can expect similar level of accuracy at zero stress as at large stress.

DFPT calculations of phonon instabilities and ideal strength have been performed for Al³² and Si³³. Recently, there have been a number of experimental^{34,35} and theoretical^{36,37} studies of phonon dispersion in graphene, which affirmed the accuracy of the DFPT approach. However, none have dealt with the ideal strength connection.

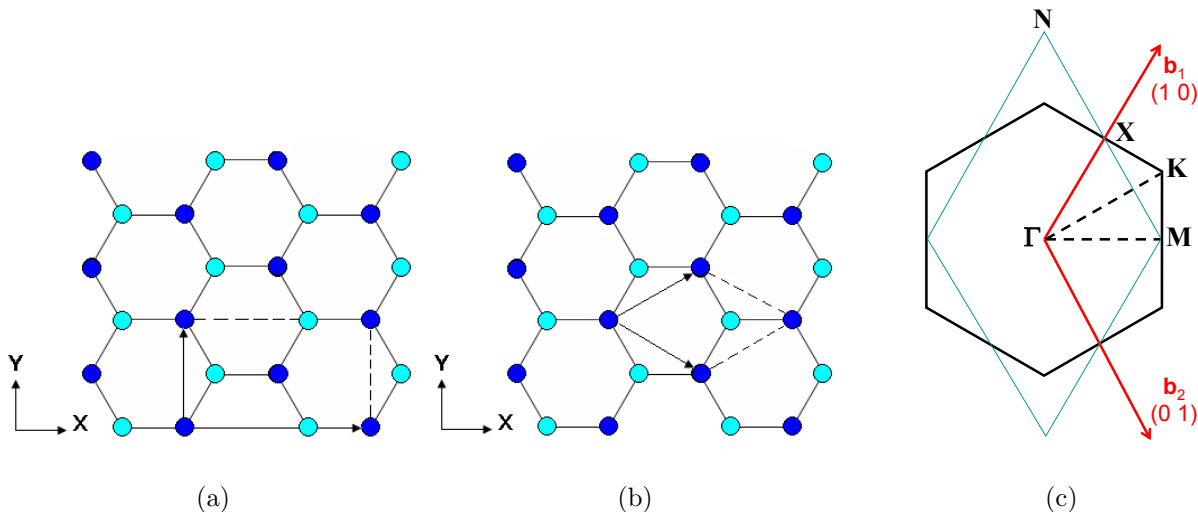


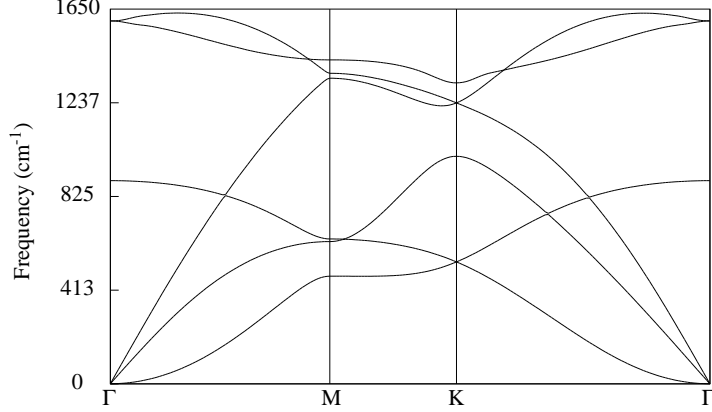
FIG. 1: (a) 4-atom unit cell for stress-strain calculations. (b) 2-atom primitive cell for phonon calculations. (c) Primitive cell of the reciprocal lattice and the first Brillouin zone.

We performed our calculations using planewave density functional theory (DFT) program ABINIT³⁸, within local density approximation (LDA). The Troullier-Martins norm-

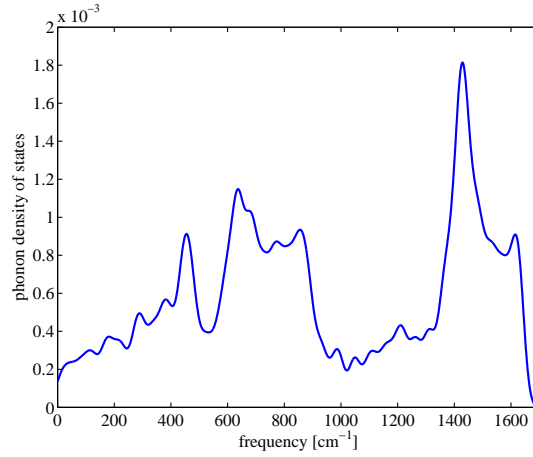
conserving pseudopotential³⁹ was used for carbon, with a planewave kinetic energy cutoff of 1633 eV. The stress-strain calculations are performed in the 4-atom unit cell, shown in Fig. 1(a). The supercell height $Z = 8 \text{ \AA}$ in the z -direction is much larger than the interlayer spacing of $d_0 = 3.34 \text{ \AA}$ in graphite⁴⁰ and carbon nanotubes. Brillouin zone (BZ) integration for charge density and total energy is performed with a 10×18 Monkhorst-Pack grid. We employ 0.1 eV Fermi-Dirac smearing of the occupation number around the Fermi level. Convergence studies indicate that the error in the stresses and energy due to the basis set size, smearing parameter, and \mathbf{k} -point grid density is less than 0.1 GPa and 0.5 meV, respectively. We first optimized the equilibrium carbon-carbon distance by the Broyden-Fletcher-Goldfarb-Shanno (BFGS) method, and obtained a value of $R_{CC} = 1.4148 \text{ \AA}$, which is only slightly different ($\leq 0.5\%$) from the experimental value of 1.419 \AA ⁴⁰.

Fig. 1(c) shows the reciprocal lattice of graphene sheet and its first Brillouin zone. For the DFPT phonon calculations, we used a 2-atom primitive cell (Fig. 1(b)) and a 20×20 \mathbf{k} -grid to map out all the possible instabilities. The results at zero stress along $\Gamma - M - K - \Gamma$ are shown in Fig. 2(a). Our results are almost identical to those of Dubay³⁶ and Wirtz³⁷. The lowest branch near Γ , $\omega^2 = \kappa k^4$, describes free bending wave of the graphene sheet at zero stress, where κ is proportional to the bending modulus of the sheet. Such free bending wave is absent in 3D crystals. *It introduces a finite density of states at zero frequency, as shown in Fig. 2(b).* According to shell elasticity, under a finite tensile stress $\sigma > 0$, this bending wave branch will turn into $\omega^2 = \kappa k^4 + \lambda \sigma k^2$ near Γ , thus no longer looks fundamentally different from the other phonon branches. *So under a non-zero tensile stress, we would expect the phonon density of states to approach 0 as the frequency $\rightarrow 0$.*

We then apply a series of incremental tensile strains on the supercell, and simultaneously relax the other stress components to zero (Poisson contraction under uniaxial tension). Uniaxial tension was applied in the x -direction and y -direction (Fig. 1), respectively. The x -direction is the nearest-neighbor C-C bonding direction. Pulling in the x -direction corresponds to pulling a zigzag nanotube of chirality $(n, 0)$, and the Poisson effect corresponds to elastic shrinking of the circumferential length of the zigzag nanotube in tension. The y -direction is the 2nd-nearest-neighbor direction. Pulling in the y -direction corresponds to pulling an armchair nanotube of chirality (n, n) , and the Poisson effect then corresponds to elastic shrinking of the armchair nanotube diameter under tension. Since the graphene primitive cell contains two atoms, there is an additional internal relative displacement be-



(a)



(b)

FIG. 2: DFPT calculated (a) phonon dispersion and (b) density of states of graphene sheet at zero stress. Note that the free bending wave $\omega^2 = \kappa k^4$ near Γ in (a) introduces a finite density of states at zero frequency in (b).

yond the affine displacements, and the Hellmann-Feynman forces need to be relaxed to zero at every strain.

Here we want to make a distinction between the calculated *supercell stress* and *equivalent stress*. The equilibrium interlayer spacing $d_0 = 3.34 \text{ \AA}$ of graphite and carbon nanotubes in nature is established through van der Waals interactions, which have minimal effect on the in-plane covalent carbon-carbon interactions. However, LDA is known to have artifacts treating the weak van der Waals interactions. Therefore in our calculations we have artificially set the supercell height to $Z = 8 \text{ \AA}$. The supercell stress computed from ABINIT is derived from linear response theory in the same vein as DFPT⁴¹, and is by default averaged over the

entire supercell volume. To make connections with experiments¹⁶ and other calculations^{42–44}, however, we need to rescale the *supercell stress* by Z/d_0 , to obtain the *equivalent stress*. The idea is that graphene should be nominally considered a continuum plate of constant thickness d_0 (with no Poisson’s contraction in the z -direction) in the context of continuum mechanics. Thus, a single-walled carbon nanotube (SWCNT) is by convention regarded as a hollow pipe rather than a full cylinder. This convention *is significant* when discussing the bending and buckling behavior of SWCNT⁴⁵, as well as the mechanics of MWCNT¹⁶.

Previous planewave DFT calculation by Ogata and Shibutani⁴⁶ indicated that peak stress of 107.4 GPa may be achieved in (10, 0) zigzag SWCNT at a critical strain 0.208, and peak stress of 114.6 GPa may be achieved in (8, 8) armchair SWCNT at a critical strain 0.295, if the nanotube could maintain its lattice structure on the strain paths. Because only a single unit cell was employed in the nanotube axis direction, the calculation was not able to detect any $\mathbf{k} \neq 0$ phonon instability. Mielke et al.⁴⁷ and Khare et al.⁴⁸ performed semi-empirical quantum mechanical calculations (PM3) with larger numbers of atoms. They predicted failure stress 124 GPa at a critical strain 0.20 for (10, 0) zigzag SWCNT, and failure stress 135 GPa at a critical strain 0.30 for the (5, 5) armchair SWCNT, respectively. Such calculations potentially can capture $\mathbf{k} \neq 0$ phonon instability. However the results were not analyzed this way.

III. RESULTS AND DISCUSSIONS

Fig. 3 shows the DFT calculated stress-strain curve and finite-deformation Poisson’s ratio of graphene. Here, strain is defined as $\varepsilon \equiv L/L_0 - 1$, and stress σ is the Cauchy stress⁴⁹, assuming the nominal plate thickness $d_0 = 3.34 \text{ \AA}$ is independent of ε . The finite-deformation Poisson’s ratio is defined as $\nu \equiv -\varepsilon(\text{lateral})/\varepsilon(\text{pulling})$, where $\varepsilon(\text{lateral})$ is the in-plane shrinkage perpendicular to the pulling axis. At small strains, graphene has isotropic in-plane elastic response, with Young’s modulus $E = 1050 \text{ GPa}$ and Poisson’s ratio $\nu = 0.186$ assessed from our DFT-LDA results. These are in good agreement with previous DFT calculations⁵⁰. At large strains the lattice symmetry is broken, and the x -strain elastic response becomes distinct from the y -strain elastic response.

$\nu(\varepsilon)$ ’s have a noticeable downward trend at large strain, indicating gradual saturation of the amount of Poisson contraction. The maximum Cauchy stress for uniaxial tension in x

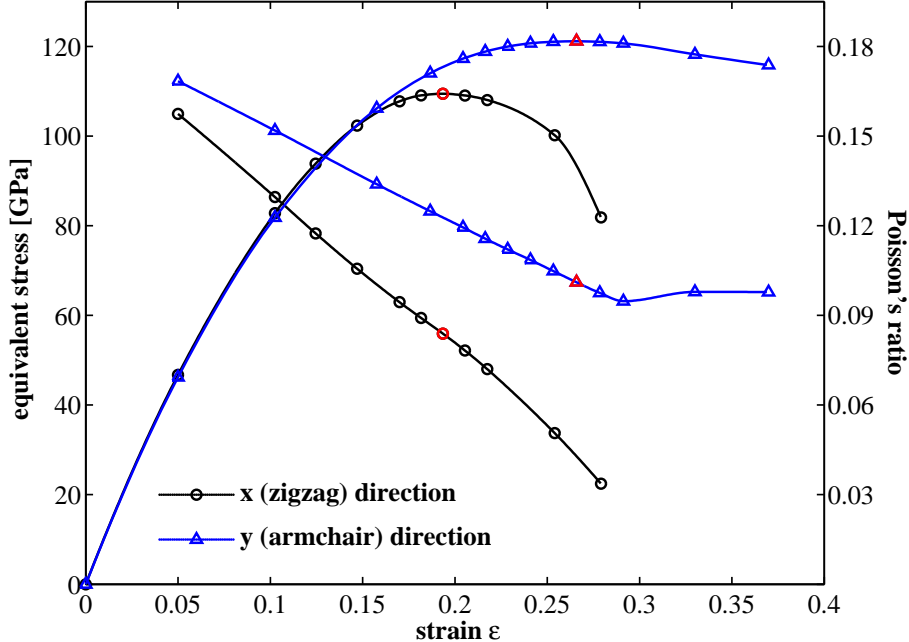


FIG. 3: The curves connected to the origin are the equivalent tensile stress ($d_0 = 3.34 \text{ \AA}$) versus uniaxial strain in the x - and y -direction, respectively. The lines with initially negative slopes (scale labels to the right) are the finite-deformation Poisson's ratios as functions of the uniaxial strain in the x - and y -direction, respectively. The red circles and triangles indicate the condition where peak stress could be attained for zigzag and armchair nanotube, respectively.

(relevant for zigzag nanotubes) is 110 GPa, at $\varepsilon_{xx} = 0.194$, $\varepsilon_{yy} = -0.016$. Thus, we should expect no more than 1.6% shrinkage in the zigzag nanotube diameter when pulled to failure at low temperatures, in agreement with experimental observations¹⁶. The predicted peak strength is in reasonable agreement with the earlier DFT estimate of 107.4 GPa at critical strain 0.208 for a zigzag nanotube⁴⁶.

Compared to being pulled in the x -direction, graphene is somewhat stronger in the y -direction (relevant for armchair nanotubes), with maximum Cauchy stress 121 GPa, at $\varepsilon_{yy} = 0.266$, $\varepsilon_{xx} = -0.027$. Thus, we predict the armchair nanotubes to be 10% stronger than the zigzag nanotubes, and can withstand 37% larger strain, with maximum diameter contraction of 2.7% (elastic) before failure at low temperatures. This peak strength is consistent with the earlier DFT estimate of 114.6 GPa at critical strain 0.295 for an armchair nanotube⁴⁶.

While Fig. 3 provides rough indication of the low-temperature strength of graphene-based nanostructures, they do not theoretically *guarantee* that the peak stresses can be *attained*,

because finite- \mathbf{k} phonon instabilities could intervene on the strain path and disrupt the homogeneous lattice structure before the peak stress is ever achieved (the instability is not soft elastic wave in nature²⁴). For instance, Clatterbuck et al. showed that in face-centered cubic aluminum, under $\langle 110 \rangle$, $\langle 100 \rangle$, $\langle 111 \rangle$ uniaxial tension as well as relaxed $\langle 11\bar{2} \rangle \{111\}$ shear, the onset of finite- \mathbf{k} phonon instabilities all occur *before* the peak stress. It is therefore imperative for us to check the stability of all phonons on the strain path, using the DFPT phonon calculations. We take the “carpet bombing” approach, that is to say we check all \mathbf{k} -points in the irreducible BZ, on a two-dimensional grid.

The results for uniaxial tension in x are shown in Fig. 4. At $\varepsilon_{xx} = 0.18$, there is no indication of phonon instability (Fig. 4(a)), that is, all of the phonon frequencies shown are positive, but significant phonon softening (lowering of the frequencies) has occurred compared to Fig. 2, except for the bending wave branch which stiffens in tension. *Also, as shown in Fig. 4(b), a narrow phonon band gap appears around 900 cm^{-1} , which might be a useful signature to spectroscopically determine highly stressed carbon nanotubes.*

Fig. 4(c) indicates that phonon instability does occur at $\varepsilon_{xx} = 0.194$, $\sigma_{xx} = 110 \text{ GPa}$, along the $\mathbf{k} = q(\mathbf{b}_1 + \mathbf{b}_2) = k\mathbf{e}_x$ direction. Blowup view (Fig. 4(d)) indicates that the instability is of long-wave nature, near Γ . The initial slope of the dispersion curve is imaginary. When this happens the material is unstable with respect to incremental tensile strain and is thus elastically unstable. To make sure this long wave at $\varepsilon_{xx} = 0.194$ is the first instance of phonon instability on the strain path, Fig. 4(e) shows the entire Brillouin zone instead of just the selected cuts. All phonon frequencies on the two-dimensional grid are positive, except for the two grid points near the zone center. Thus the first instability is elastic in nature, which means the peak stress and strain can be attained at 0K, $\sigma_{I,xx} = 110 \text{ GPa}$, $\varepsilon_{I,xx} = 0.194$.

For such situation, a general theory exists about how a linear instability of long waves can lead to dynamic nucleation of defect singularities like dislocations or cracks^{24,25}. *In simple crystals, if \mathbf{w} is more perpendicular to \mathbf{k} , then the unstable wave is transverse, i.e. it is a soft shear wave. It is very likely then that a dislocation loop or a twin embryo would be nucleated. If however \mathbf{w} is more parallel to \mathbf{k} , then the unstable wave is longitude, and a microcrack is likely to result.*

The eigenvector of the dynamical matrix (Fig. 4(f)) indicates this soft phonon mode at $\varepsilon_{I,xx} = 0.194$ is a longitudinal wave, with polarization displacement \mathbf{w} parallel to $\mathbf{k} \parallel \mathbf{e}_x$,

and thus should lead to the nucleation of micro-crack when $\sigma_{1,xx} = 110$ GPa is attained at $T = 0$ K. This is in agreement with Dumitrica et al.'s analysis⁴³, that at low temperatures the failure mode of zigzag nanotubes is brittle cleavage fracture. Only when the temperature is high enough ($T > T_D/2 \sim 500$ K) can zigzag nanotubes deform plastically at laboratory strain rates via the nucleation and migration of Stone-Wales 5/7 defects^{43,45}. At such elevated temperatures, the ideal strength (athermal strength) is no longer a good indicator of the prevalent deformation mechanism; one must also look at thermally activated processes and their activation volumes^{7,28,51}, which is beyond the scope of this paper.

The DFPT phonon calculations for uniaxial tension in y (armchair nanotubes) are shown in Fig. 5. The results are similar to uniaxial tension in x , *except that the phonon band gap is now much wider. This gap centered around 1200 cm^{-1} would be a good diagnostic signature of highly stressed carbon nanotubes.* We predict longitudinal elastic wave instability for armchair nanotubes, with $\mathbf{w} \parallel \mathbf{k} \parallel \mathbf{e}_y$, at $\varepsilon_{1,yy} = 0.266$ and $\sigma_{1,yy} = 121$ GPa, which usually suggests brittle cleavage fracture behavior²⁵. Analysis of the relationship between \mathbf{w} and atomic geometry (Fig. 5(f)), however, reveals a small difference. While \mathbf{w} was parallel to the highest-load nearest-neighbor bonds in Fig. 4(f), it now has a $\sim 30^\circ$ angle to the highest-load bonds in Fig. 5(f). This means in a longitudinal displacement field like $\mathbf{u}(\mathbf{x}) = \mathbf{w}e^{i\mathbf{k}\cdot\mathbf{x}}$, while the highest-load bonds in Fig. 4(f) sustain stretching but not rotation, the highest-load bonds will sustain both bond stretching and bond rotation in Fig. 5(f). Because the Stone-Wales transformation involves bond rotation⁴⁵, it is not absolutely clear whether the linear instability of Fig. 5(f) will lead to bond cleavage first or localized Stone-Wales transformation first. *Such complication arises because graphene has a 2-atom primitive cell and the response to macroscopic strain is non-affine.*

Dumitrica et al. predicted localized Stone-Wales transformation and plastic deformation for armchair nanotubes at low temperatures⁴³ ($T=1\text{K}$, 300K , and 600K) in a stress ramp-up experiment. We note that experimentally, there is not yet evidence of low-temperature plastic deformation of carbon nanotubes of any chirality. Demczyk et al. found no plastic narrowing of the nanotubes immediately before failure¹⁶. On the other hand, it is possible to fracture *quickly (with respect to human timescale)* after the 5/7 defects have been nucleated⁵² *or perhaps after the aggregation of several 5/7 defects*⁵³. Thus experiments to date provide no concrete evidence either for or against initial Stone-Wales transformation at low temperature and laboratory strain rates. It is reasonable however to interpret our DFPT results as

suggesting that both the zigzag and armchair nanotubes are intrinsically capable of brittle cleavage fracture at $T = 0\text{K}$, due to the longitudinal elastic wave nature of the first soft phonons when subjected to tension.

Acknowledgments

F.L. acknowledges support from the National Science Foundation of China (10425105) and the National Basic Research Program (2005CB321704). The calculations were performed on LSSC-II at the State Key Laboratory of Scientific and Engineering Computing, Chinese Academy of Sciences. P.M. acknowledges support under the National Natural Science Foundation of China (10571172) and the National Basic Research Program (2005CB321704). J.L. acknowledges support by DoE DE-FG02-06ER46330, NSF DMR-0502711, ONR N00014-05-1-0504, AFOSR, and Ohio Supercomputer Center.

* Electronic address: li.562@osu.edu

- ¹ T. Li, J. W. Morris, N. Nagasako, S. Kuramoto, and D. C. Chrzan, *Phys. Rev. Lett.* **98**, 105503 (2007).
- ² J. Pokluda, M. Cerny, P. Sandera, and M. Sob, *J. Comput-Aided Mater. Des.* **11**, 1 (2004).
- ³ S. Ogata, J. Li, and S. Yip, *Science* **298**, 807 (2002).
- ⁴ S. Ogata, J. Li, N. Hirotsuki, Y. Shibutani, and S. Yip, *Phys. Rev. B* **70**, 104104 (2004).
- ⁵ R. Peierls, *Proc. Phys. Soc* **52**, 34 (1940).
- ⁶ F. R. N. Nabarro, *Proc Phys Soc Lond* **59**, 256 (1947).
- ⁷ J. Li, *MRS Bull.* **32**, 151 (2007).
- ⁸ K. S. Kumar, H. Van Swygenhoven, and S. Suresh, *Acta Mater.* **51**, 5743 (2003).
- ⁹ C. A. Volkert, E. T. Lilleodden, D. Kramer, and J. Weissmuller, *Appl. Phys. Lett.* **89**, 061920 (2006).
- ¹⁰ J. R. Greer and W. D. Nix, *Phys. Rev. B* **73**, 245410 (2006).
- ¹¹ A. Gouldstone, N. Chollacoop, M. Dao, J. Li, A. M. Minor, and Y.-L. Shen, *Acta Mater.* **55**, 4015 (2007).
- ¹² P. R. Chidambaram, C. Bowen, S. Chakravarthi, C. Machala, and R. Wise, *IEEE Trans. Elec-*

- tron Devices **53**, 944 (2006).
- ¹³ M. R. Falvo, G. J. Clary, R. M. Taylor, V. Chi, F. P. Brooks, S. Washburn, and R. Superfine, Nature **389**, 582 (1997).
- ¹⁴ M. F. Yu, B. S. Files, S. Arepalli, and R. S. Ruoff, Phys. Rev. Lett. **84**, 5552 (2000).
- ¹⁵ W. Ding, L. Calabri, K. M. Kohlhaas, X. Chen, D. A. Dikin, and R. S. Ruoff, Exp. Mech. **47**, 25 (2007).
- ¹⁶ B. G. Demczyk, Y. M. Wang, J. Cumings, M. Hetman, W. Han, A. Zettl, and R. O. Ritchie, Mater. Sci. Eng. A **334**, 173 (2002).
- ¹⁷ A. H. Barber, R. Andrews, L. S. Schadler, and H. D. Wagner, Appl. Phys. Lett. **87**, 203106 (2005).
- ¹⁸ A. Marquez-Lucero, J. A. Gomez, R. Caudillo, M. Miki-Yoshida, and M. Jose-Yacaman, Small **1**, 640 (2005).
- ¹⁹ R. Saito, G. Dresselhaus, and M. S. Dresselhaus, *Physical properties of carbon nanotubes* (Imperial College Press, London, 1998).
- ²⁰ S. Stankovich, D. A. Dikin, G. H. B. Dommett, K. M. Kohlhaas, E. J. Zimney, E. A. Stach, R. D. Piner, S. T. Nguyen, and R. S. Ruoff, Nature **442**, 282 (2006).
- ²¹ M. T. Dove, *Introduction to Lattice Dynamics* (Cambridge University Press, 1993).
- ²² A. Maradudin, E. Montroll, G. Weiss, and I. Ipatova, *Theory of lattice dynamics in the harmonic approximation* (Academic Press, New York, 1971), 2nd ed.
- ²³ T. Tohei, A. Kuwabara, F. Oba, and I. Tanaka, Phys. Rev. B **73**, 064304 (2006).
- ²⁴ J. Li and S. Yip, CMES-Comp. Model. Eng. Sci. **3**, 219 (2002).
- ²⁵ J. Li, A. H. W. Ngan, and P. Gumbsch, Acta Mater. **51**, 5711 (2003).
- ²⁶ W. N. E and P. B. Ming, Arch. Ration. Mech. Anal. **183**, 241 (2007).
- ²⁷ Y. Umeno, A. Kushima, T. Kitamura, P. Gumbsch, and J. Li, Phys. Rev. B **72**, 165431 (2005).
- ²⁸ T. Zhu, J. Li, A. Samanta, A. Leach, and K. Gall, submitted (2007).
- ²⁹ S. V. Dmitriev, T. Kitamura, J. Li, Y. Umeno, K. Yashiro, and N. Yoshikawa, Acta Mater. **53**, 1215 (2005).
- ³⁰ S. Baroni, S. de Gironcoli, A. Dal Corso, and P. Giannozzi, Rev. Mod. Phys. **73**, 515 (2001).
- ³¹ L. J. Porter, J. Li, and S. Yip, J. Nucl. Mater. **246**, 53 (1997).
- ³² D. M. Clatterbuck, C. R. Krenn, M. L. Cohen, and J. W. Morris, Phys. Rev. Lett. **91**, 135501 (2003).

- ³³ S. M. M. Dubois, G. M. Rignanese, T. Pardoen, and J. C. Charlier, Phys. Rev. B **74**, 235203 (2006).
- ³⁴ A. Gruneis, R. Saito, T. Kimura, L. G. Cancado, M. A. Pimenta, A. Jorio, A. G. Souza, G. Dresselhaus, and M. S. Dresselhaus, Phys. Rev. B **65**, 155405 (2002).
- ³⁵ J. Maultzsch, S. Reich, C. Thomsen, H. Requardt, and P. Ordejon, Phys. Rev. Lett. **92**, 075501 (2004).
- ³⁶ O. Dubay and G. Kresse, Phys. Rev. B **67**, art. no. (2003).
- ³⁷ L. Wirtz and A. Rubio, Solid State Commun. **131**, 141 (2004).
- ³⁸ X. Gonze, J. M. Beuken, R. Caracas, F. Detraux, M. Fuchs, G. M. Rignanese, L. Sindic, M. Verstraete, G. Zerah, F. Jollet, et al., Comput. Mater. Sci. **25**, 478 (2002).
- ³⁹ N. Troullier and J. L. Martins, Phys. Rev. B **43**, 1993 (1991).
- ⁴⁰ Y. Baskin and L. Meyer, Phys Rev **100**, 544 (1955).
- ⁴¹ R. M. Martin, *Electronic Structure: Basic Theory and Practical Methods* (Cambridge University Press, Cambridge, 2004).
- ⁴² T. Dumitrica, T. Belytschko, and B. I. Yakobson, J. Chem. Phys. **118**, 9485 (2003).
- ⁴³ T. Dumitrica, M. Hua, and B. I. Yakobson, Proc. Natl. Acad. Sci. U. S. A. **103**, 6105 (2006).
- ⁴⁴ P. W. Chung, Phys. Rev. B **73**, 075433 (2006).
- ⁴⁵ H. Mori, S. Ogata, J. Li, S. Akita, and Y. Nakayama, Phys. Rev. B **74**, 165418 (2006).
- ⁴⁶ S. Ogata and Y. Shibusaki, Phys. Rev. B **68**, 165409 (2003).
- ⁴⁷ S. L. Mielke, D. Troya, S. Zhang, J. L. Li, S. P. Xiao, R. Car, R. S. Ruoff, G. C. Schatz, and T. Belytschko, Chem. Phys. Lett. **390**, 413 (2004).
- ⁴⁸ R. Khare, S. L. Mielke, J. T. Paci, S. L. Zhang, R. Ballarini, G. C. Schatz, and T. Belytschko, Phys. Rev. B **75**, 075412 (2007).
- ⁴⁹ T. Zhu, J. Li, K. J. Van Vliet, S. Ogata, S. Yip, and S. Suresh, J. Mech. Phys. Solids **52**, 691 (2004).
- ⁵⁰ K. N. Kudin, G. E. Scuseria, and B. I. Yakobson, Phys. Rev. B **64**, 235406 (2001).
- ⁵¹ T. Zhu, J. Li, A. Samanta, H. G. Kim, and S. Suresh, Proc. Natl. Acad. Sci. U. S. A. **104**, 3031 (2007).
- ⁵² J. Song, H. Jiang, D. L. Shi, X. Q. Feng, Y. Huang, M. F. Yu, and K. C. Hwang, Int. J. Mech. Sci. **48**, 1464 (2006).
- ⁵³ D. Troya, S. L. Mielke, and G. C. Schatz, Chem. Phys. Lett. **382**, 133 (2003).

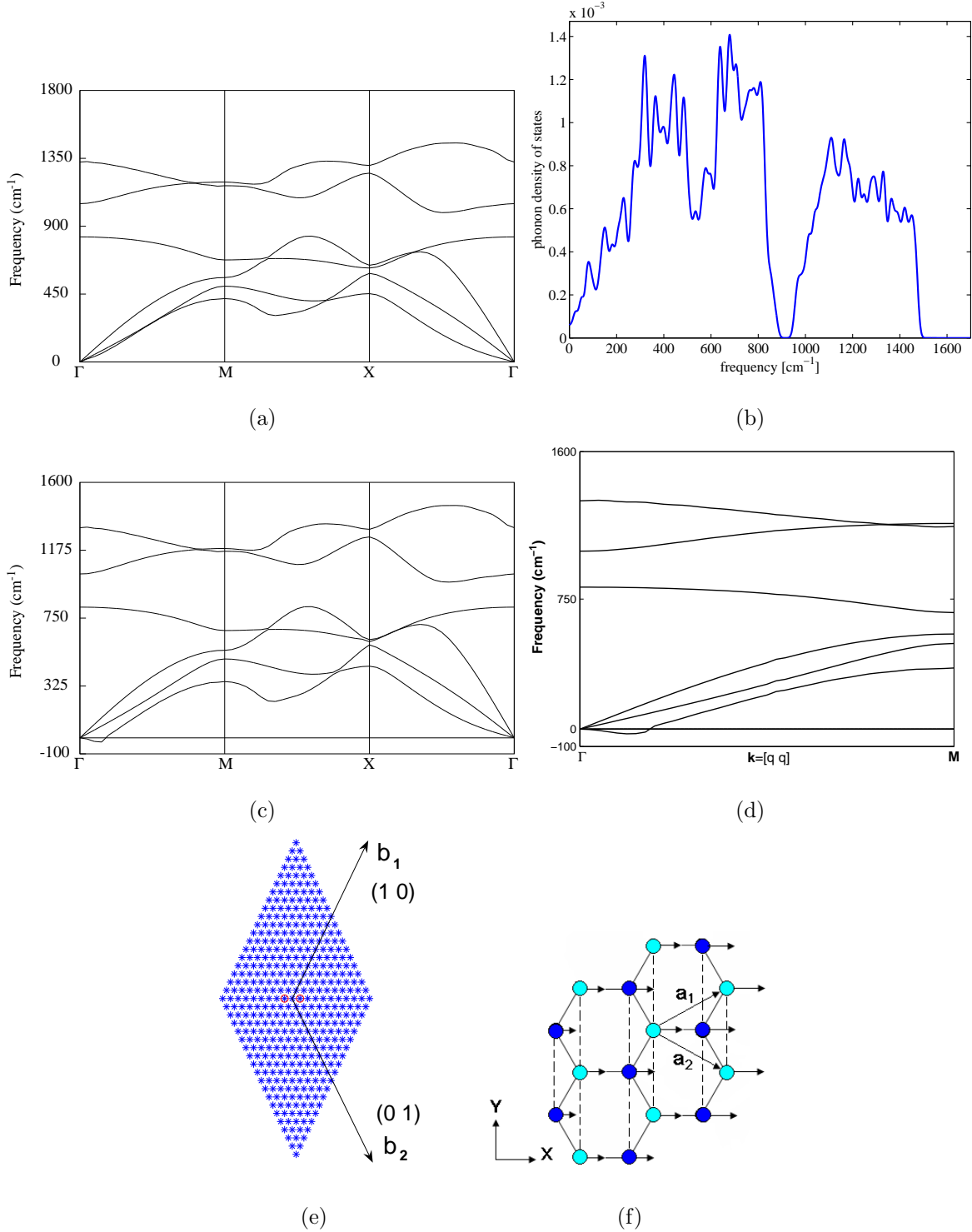


FIG. 4: (a) Phonon dispersion and (b) density of states of graphene at $\varepsilon_{xx} = 0.18$. There is no soft mode yet. (c) Phonon dispersion at $\varepsilon_{xx} = 0.194$, $\sigma_{xx} = 110$ GPa. (d) Blowup of the unstable branch along $\mathbf{k} = q(\mathbf{b}_1 + \mathbf{b}_2) = k\mathbf{e}_x$. (e) Scan of the entire Brillouin zone at $\varepsilon_{xx} = 0.194$ to make sure that (d) is the first phonon instability. \otimes indicates imaginary and $*$ indicates real frequency. (f) The unstable eigenvector corresponding to the soft mode at $\varepsilon_{xx} = 0.194$.

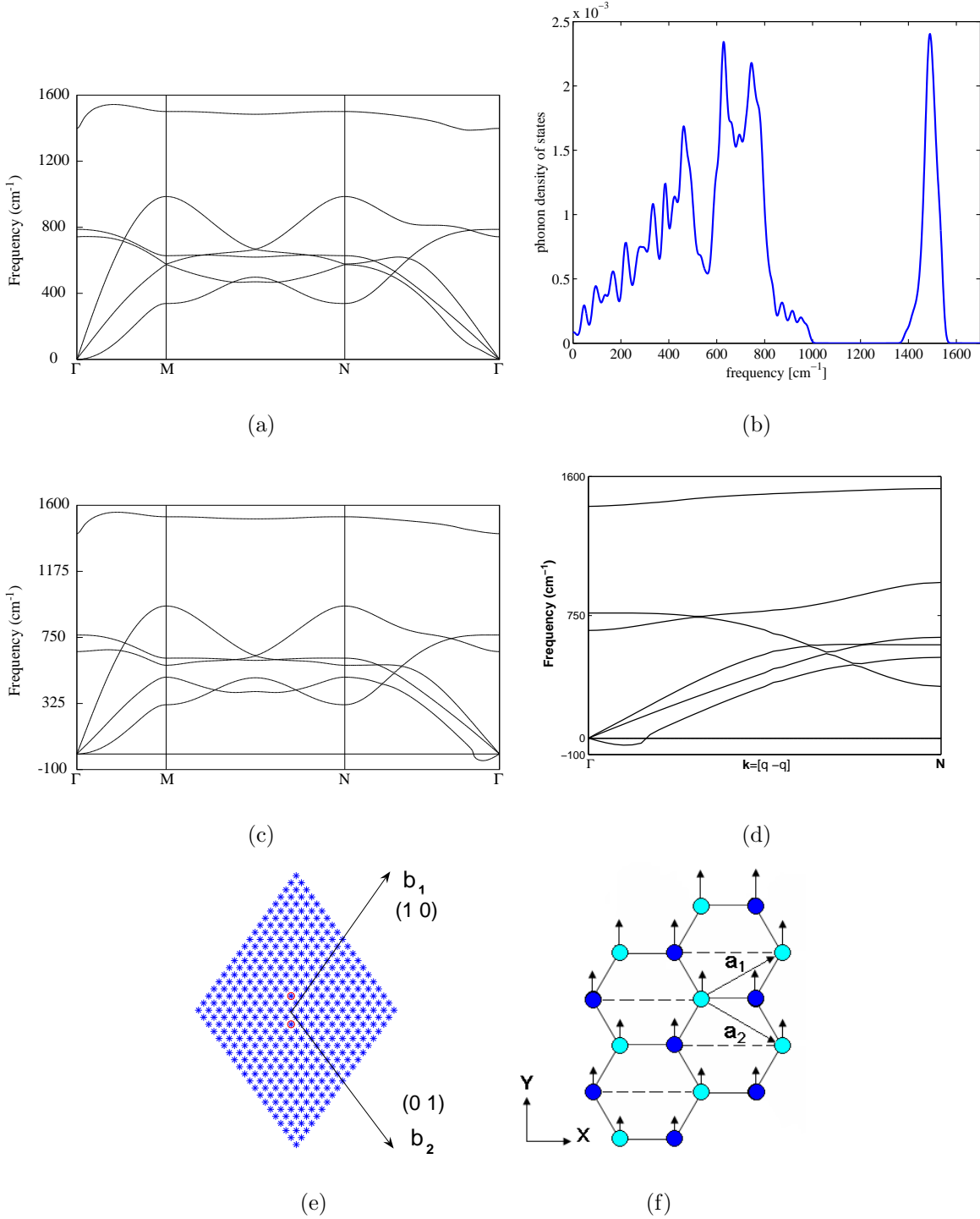


FIG. 5: (a) Phonon dispersion and (b) density of states of graphene at $\varepsilon_{yy} = 0.24$. There is no soft mode yet. (c) Phonon dispersion at $\varepsilon_{yy} = 0.266$, $\sigma_{yy} = 121$ GPa. (d) Blowup of the unstable branch along $\mathbf{k} = q(\mathbf{b}_1 - \mathbf{b}_2) = k\mathbf{e}_y$. (e) Scan of the entire Brillouin zone at $\varepsilon_{yy} = 0.266$ to make sure (d) is the first phonon instability. \otimes indicates imaginary and $*$ indicates real frequency. (f) The unstable eigenvector corresponding to the soft mode at $\varepsilon_{yy} = 0.266$.